Bone 127 (2019) 646–655

Contents lists available at ScienceDirect

Bone

journal homepage: www.elsevier.com/locate/bone

Full Length Article

A novel transgenic murine model with persistently brittle bones simulating osteogenesis imperfecta type I

Yi Liu[a,1], Jianhai Wang[a,1], Shuo Liu[a], Mingjie Kuang[b], Yaqing Jing[a], Yuxia Zhao[a], Zihan Wang[a], Guang Li[a,*]

[a] Department of Genetics, School of Basic Medical Sciences, Tianjin Medical University, Tianjin, People's Republic of China
[b] Department of Orthopedics, Tianjin Medical University General Hospital, Tianjin, People's Republic of China

ARTICLE INFO

Keywords:
Transgenic animal model
Osteogenesis imperfecta
Brittle bone
Osteogenic differentiation
Hippo/YAP

ABSTRACT

Osteogenesis imperfecta (OI) type I caused by the null allele of *COL1A1* gene is in the majority in clinical OI cases. Currently, heterozygous Mov-13 mice generated by virus insertion in the first intron of *col1a1* is the exclusive model to modulate OI type I, in spite of the gradually recovered bone mineral and mechanical properties. A newly designed heterozygous *col1a1* $^{\pm 365}$ OI mouse was produced in the present study by partial exons knockout (exon 2-exon 5, 365 nt of mRNA) using CRISPR/Cas9 system. The deletion resulted in generally large decrease in type I collagen synthesis due to frameshift mutation and premature chain termination, closely mimicking the pathogenic mechanism in affected individuals. And the strain possessed significantly sparse mineral scaffolds, bone loss, lowered mechanical strength and broken bone metabolism by 8 and 20 weeks compared to their littermates, suggesting a sustained skeletal weakness. Notably, the remarkable down-regulation of Yes-associated protein (YAP), one of the key coactivator in Hippo signaling pathway, was first found both in the femur and adipose derived mesenchymal stem cells (ADSCs) under osteogenic differentiation of *col1a1* $^{\pm 365}$ mice, which might be responsible for the reduced osteogenic potential and brittle bones. Still, further research was needed in order to illuminate the underlying mechanism.

1. Introduction

Osteogenesis imperfecta (OI), also known as brittle bone disease, is a congenital disorder with the skeletal system mainly affected. Individuals suffering from OI often manifest low bone mass and recurrent fractures [1]. Weight-bearing bones especially femurs tend to be susceptibly involved. About 85% OI patients are caused by autosomal dominant mutations in *COL1A1* or *COL1A2* gene which encodes procollagen α1 (pro-α1(I)) or pro-α2(I) chain of type I collagen [2]. Among them, OI type I (the mild type according to Sillence classification) resulted from null mutation of *COL1A1* is the most common type in clinical practice [3,4].

OI was first associated with collagen abnormality in early 1980s [5]. Great progress in genomic approaches effectually accelerated the understanding of OI in the last few decades. Previous studies including ours indicated that nonsense mediated decay (NMD) due to premature termination codons caused by *COL1A1* null mutation was primarily responsible for OI type I [4,6–8]. The degradation of mutant transcripts and quantitative loss of collagen reduced bone mass and strength, resulting in the mild form of OI. Besides the genetic screening, animal models especially OI mice also contributed a lot in related research.

To date, heterozygous Mov-13 mouse (MOV $13^{+/-}$) proposed in 1992 is the only model to stimulate the phenotype of OI type I [9]. The strain was generated by Moloney murine leukemia virus (M-MuLV) insertion in the first intron of *col1a1* to prevent RNA polymerase binding and further block transcription initiation [10]. The heterozygotes produced about 50% less but structurally normal type I collagen and manifested bone brittleness [11]. Jeffrey B. et al demonstrated an unexpected improvement of bending strength in 8-week old mice probably due to osteoblasts proliferation and collagen synthesis increase on the periosteal surface of long bones [12]. And by 15 weeks, the load-bearing capacity and mineralization returned to normal level [12]. Although the skeletal adaptation of Mov-13 mice is somewhat similar to the performance of adolescent and adult patients, to further explore the molecular mechanism and seek novel possible targets, the model with stable phenotype is still important and necessary.

* Corresponding author at: Department of Genetics, School of Basic Medical Sciences, Tianjin Medical University, 22 Qixiangtai Road, Heping District, Tianjin 300070, People's Republic of China.
E-mail address: lig@tmu.edu.cn (G. Li).
[1] These authors contributed equally to this work.

https://doi.org/10.1016/j.bone.2019.07.021
Received 14 February 2019; Received in revised form 27 June 2019; Accepted 17 July 2019
Available online 29 July 2019

Here, we reported a newly designed *col1a1* knockout (*col1a1* $^{\pm 365}$) OI mouse with exon 2- exon 5 (365 nt of mRNA) deletion by CRISPR/Cas9 system. The partial exons knockout resulted in frameshift mutation and premature chain termination, closely mimicking clinical cases of OI type I [8]. The heterozygous *col1a1* $^{\pm 365}$ mice harbored an obvious femoral collagen reduction accompanied with significantly sparse mineral scaffolds, low bone mass and load strength by 8 and 20 weeks when compared with their normal litters, suggesting a sustained skeletal weakness. But similar to Mov-13 mice, none of spontaneous fractures were found by 20 weeks. Notably, the remarkable down-regulation of Yes-associated protein (YAP), one of the core members in Hippo signaling, was first found both in femurs and adipose derived mesenchymal stem cells (ADSCs) under osteogenic induction of *col1a1* $^{\pm 365}$ mice. The significance of Hippo pathway in osteogenesis and bone homeostasis has aroused wide concern and increasing evidence indicates that it plays a pivotal role in osteoclasts and osteoblasts balancing in postnatal bone remodeling [13]. YAP and TAZ combinatorially promote bone development through regulation of osteoblast activity, matrix quality and osteoclastic remodeling [14]. And Jin-Xiu Pan et al reported that conditionally knocking out YAP in bone marrow derived mesenchymal stem cells (BMSCs) reduced cell proliferation and osteoblast differentiation and the YAP$^{Ocn\text{-}Cre}$ mice suffered from a trabecular bone loss [15]. In other words, reduced YAP protein levels directly/causally contributes to the weakened osteogenesis and brittle bones, which might exert the same effect on *col1a1* $^{\pm 365}$ mice. Still, further research to uncover the underlying mechanism was required.

2. Materials and methods

2.1. Animals

The *col1a1* $^{\pm 365}$ mice (C57B/L6 background) were developed by *col1a1* knockout via CRISPR/Cas9 system and generated in Nanjing Medical Research Institute of Nanjing University. In brief, Cas9 mRNA and sgRNA targeting murine *col1a1* gene (NM_007742.4) were co-injected into zygotes. Cas9 endonuclease cleaved the sequence under the direction of sgRNA and created a double-strand break (DSB) which could be repaired and resulted in deletion of exon 2- exon 5 (1029 bp of DNA, 365 nt of mRNA). Sanger sequencing confirmed the 1029 bp knockout of heterozygotes.

Adult wild type (*wt*) C57BL/6 mice (8–10 weeks old) were purchased from the Laboratory Animal Center of the Academy of Military Medical Science (Beijing, China). Male heterozygous mice were mated to wild type females to provide sufficient transgenic mice. Mice were kept and handled under specific pathogen free conditions in accordance with the approval by Animal Care and Use Committee of Tianjin Medical University (TMUaMEC 2017012). The mouse tail genome was used to identify the genotype of progenies by Polymerase Chain Reaction (PCR) 2 weeks after birth. The primers (Forward: CACCTAC TGCGTAGGAGCCC, Reverse: CCCAACAGCCAGACTCTTCA) stretched across the lost exons. The growing stats including height and weight of *col1a1* $^{\pm 365}$ mice (n = 30) and their normal littermates (n = 30) were recorded. The blood and femurs were harvested for further analysis post sacrifice in different time points. Only male mice were used in the present study.

2.2. Cells

Adipose derived mesenchymal stem cells (ADSCs) were isolated from 6 weeks old *wt* (ADSCs^{wt}) and *col1a1* $^{\pm 365}$ (ADSCs $^{\pm}$ *365*) mice as described previously [16]. Cells from adipose tissues near the groin and epididymis were adherently cultured in αMEM medium (Gibco) supplemented with 20% fetal bovine serum (FBS, Gibco) and 5000 U/mL penicillin/streptomycin (Gibco). The culture medium was replaced every three days until cell confluent. Passage 3rd cells qualified by fluorescence activated cell sorting (FACS) and differentiation capacity detection were shown in the Supplemental Information (SI) in accordance with previous reports [17]. The osteogenic differentiation ability was confirmed by alkaline phosphatase (ALP, Sigma-Aldrich) staining and ALP enzymatic activity in the cultural supernatant was examined by ALP Activity Detection Kit (Beyotime) of the two kinds of ADSCs post 14 days' induction.

2.3. Micro-computed tomography (Micro-CT)

The femurs were harvested from 8 and 20 weeks old *col1a1* $^{\pm 365}$ mice (n = 6) and their *wt* littermates (n = 6). The whole bones were scanned by micro-CT (SkyScan 1276) using the high resolution SkyScan 1174 V2 system operating at 50 kV, according to manufacturer's directions. Trabecular bone parameters were measured in the distal metaphysis of the femurs. The region of interest was selected from the proximal distal growth plate where the epiphyseal cap structure completely disappeared and continued for 150 slices toward the end of the femur. Trabecular bone was separated from cortical bone with manually drawn contour lines. Cortical bone parameters were measured of femur mid-diaphysis (at the middle position). Three-dimensional (3D) reconstruction and viewing of images were conducted on CTAn software (version 1.15.4). The trabecular bone parameters calculated based on the scanning charts included bone volume/total volume (Tb. BV/TV), bone surface area/bone volume (Tb. BS/BV), trabecular thickness (Tb. Th), trabecular number (Tb. N) and trabecular spacing (Tb. Sp). For cortical bones, the thickness and area were also measured (SI).

2.4. Dual-energy X-ray absorptiometry (DXA)

Bone mineral density (BMD; gram per square centimeter, g/cm^2) and bone mineral content (BMC; gram, g) data of *wt* (n = 8) and *col1a1* $^{\pm 365}$ mice (n = 8) were acquired using Faxitron Ultrafocus DXA equipment (Faxitron Bioptics, USA) by 8 and 20 weeks. During DXA scanning, the mice were anesthetized by isoflurane inhalation, and the BMD and BMC of the whole body were calculated by the scanner software.

2.5. Bone biomechanics

The mechanical properties of femurs were measured by three-point bending analysis on a Bose ElectroForce 3100 system (Bose, USA) when mice were 8 and 20 weeks old (n = 6 for each group). Prior to testing, all bones were kept moist in gauze swabs infiltrated with PBS. The femur was loaded to failure in the anterior-posterior direction with a span length of 7 mm at a constant displacement rate of 0.5 mm/s until failure occurred. Data were collected by WinTest software at 250 data points per second for a total of 10 s. The maximum load (Newtons, N), bone stiffness (N/mm) the Post-Yield Displacement, Post-Yield Energy and Work-to-Fracture were determined from the applied load and displacement value. Structural mechanical properties, ultimate load, stiffness, displacement, and energy absorption were determined from the load-deformation curves using standard definitions [18,19].

2.6. Enzyme-linked immunosorbent assay (ELISA)

ELISA tests were used to measure serum biomarkers of bone formation and bone resorption. Mice were all fasted for > 5 h before serum collection. Peripheral blood samples collected of 8 and 20 weeks old *wt* (n = 8) and *col1a1* $^{\pm 365}$ mice (n = 8) were analyzed for the levels of procollagen type I N-terminal propeptide (PINP) and C-terminal telopeptide of type I collagen (CTX−I) using ELISA kits (Cusabio) according to the manufacturer's protocol.

2.7. Histological, immnuohistochemical and immunofluorescence staining

Femur samples were fixed with 4% paraformaldehyde, embedded in

Table 1
Primers used for qPCR detection.

Genes	Forward primer sequence	Reverse primer sequence	Product length/bp
col1a1	CCTCAGGGTATTGCTGGACAAC	CAGAAGGACCTTGTTTGCCAGG	115
runx2	TCCTGTAGATCCGAGCACCA	CTGCTGCTGTTGTTGCTGTT	163
osterix	GGCTTTTCTGCGGCAAGAGGTT	CGCTGATGTTTGCTCAAGTGGTC	139
ctgf	TGCGAAGCTGACCTGGAGGAAAC	CCGCAGAACTTAGCCCTGTATG	131
cyr61	GTGAAGTGCGTCCTTGTGGACA	CTTGACACTGGAGCATCCTGCA	122
gadph	CATCACTGCCACCCAGAAGACTG	ATGCCAGTGAGCTTCCCGTTCAG	153

runx2, Runt-related transcription factor 2; ctgf, connective tissue growth factor; cyr61, cysteine-rich angiogenic inducer 61; gadph, glyceraldehyde-3-phosphate dehydrogenase.

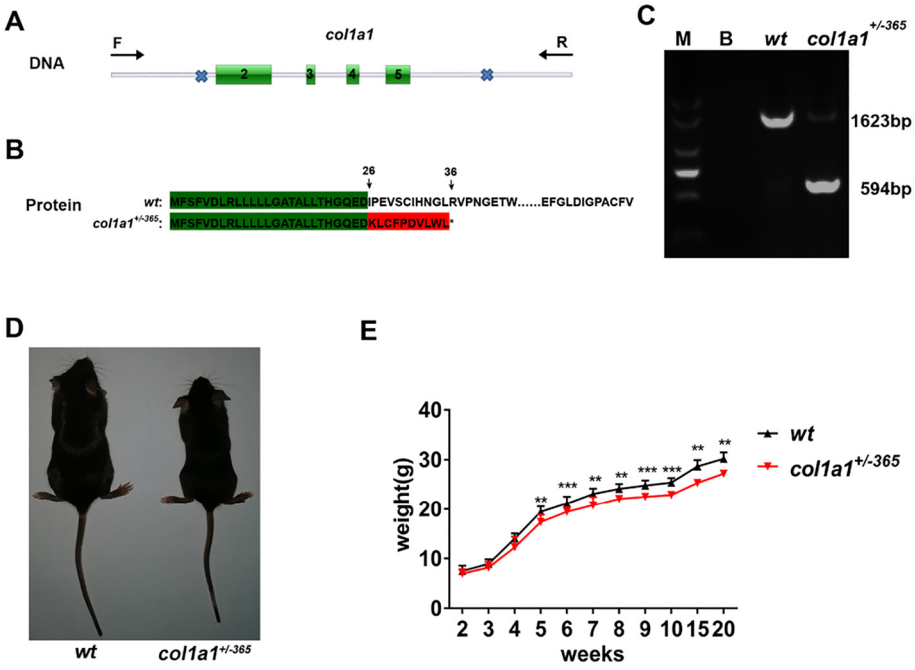

Fig. 1. The generation and identification of the transgenic murine model
A Diagram of partial exons knock-out of *col1a1*. Blue crosses were the site of Cas9 endonuclease cleavage, and the green boxes were exon 2-exon 5. F and R were primers for PCR-based genotyping. **B** The protein sequence predicting of the mutant *col1a1* allele. The deletion would cause a translational frameshift at the 26th amino acid and produce a stop codon at 36th amino acid. *: stop codon **C** Genotype identification by PCR analysis of the two kind of mice. The 1623 bp band was indicative of the *wt* allele, and the short 594 bp band of the *col1a1* $^{\pm}$ *365* allele. The heterozygous mice had one 1623 bp band and one 594 bp band. M: 1 kb DNA ladder. **D** The appearance of *wt* mice (6 weeks old) and *col1a1* $^{\pm}$ *365* mice (6 weeks old). **E** The weight growth curve of mice (n = 15 mice/group) from weaning (2 weeks) to 20 weeks of age. $^{**}p < 0.01$, $^{***}p < 0.005$. (For interpretation of the references to colour in this figure legend, the reader is referred to the web version of this article.)

paraffin following decalcification, and cut into 5-μm-thick sections by 8 weeks. Hematoxylin and Eosin (H&E) showed the histology. The osteoclastic condition was assessed by tartrate-resistant acid phosphatase (TRAP) staining. The percentage of the TRAP-positive osteoclast in contact with trabecular surface [TRAP$^+$OcS/BS (%)] and the number of TRAP-positive osteoclasts per millimeter of the trabecular surface [TRAP$^+$OcN/BS(mm)] were counted. ADSCs $^{\pm}$ *365* seeded on glass sheets with or without osteogenic induction for 3 days were incubated with YAP (Santa Cruz, 1:500), and then with Alexa Fluor 488 goat anti-rat immunoglobulin G (IgG; Molecular Probes). Cell nuclei were stained with 4′,6-diamidino-2-phenylindole (DAPI; Sigma- Aldrich). The fluorescence intensity under the same exposure time of 50 cells of each group was analyzed by ImageJ software (Table 1).

2.8. Quantitative real-time PCR (qPCR)

The transcriptional expression of *col1a1* and genes involved in osteogenic potential (*Runt-related transcription factor 2/runx2* and *osterix*) and Hippo signal pathway (*connective tissue growth factor/ctgf* and *cysteine-rich angiogenic inducer 61/cyr61*) was tested by qPCR. Total RNA of the femur tissues from 8 weeks old *wt* (n = 6) and *col1a1* $^{\pm}$ ^{365} mice (n = 6) as well as ADSCs $^{\pm}$ *365* were extracted with TRIzol reagent (Life Technologies). For each sample, 2 μg RNA was used to synthesize cDNA with the GoScript™ Reverse Transcription Mix, Oligo(dT) kit (Promega). And qPCR was performed in triplicate using SYBR Green mix kit (QIAGEN) according to the instructions. The ΔΔCt method was used for data analysis and the level of *glyceraldehyde-3-phosphate dehydrogenase* (*gapdh*) served as control. Primers designed by Primer Premier 5 software for related genes were listed in supplemental Table 1.

2.9. Western blot

The western blot analysis determined the protein levels in femurs. Protein samples were prepared by RIPA lysis buffer and separated by SDS-PAGE using 10% gels and subsequently transferred to PVDF membranes (Bio-Rad). The primary antibodies included pro-α1(I) (Abcam, 1:1000), bone gamma-carboxyglutamic acid-containing protein (Bglap, Abcam, 1:500), YAP (Santa Cruz, 1:1000) and Gapdh (Affinity, 1:2000). The secondary antibodies were diluted at a 1:2000 ratio. The relative expression compared with Gapdh was calculated by ImageJ software.

2.10. Statistical analysis

Statistical analysis was conducted in SPSS version 17.0 software (SPSS Inc., Chicago, USA). All data were presented as mean ± SEM and compared using unpaired *t*-test. Differences with p values < 0.05 were considered significant.

3. Result

3.1. Generation and identification of the col1a1 ± 365 mice

The exon 2- exon 5 of *col1a1* gene (1029 bp in DNA, 365 nt in mRNA) was deleted using CRISPR/Cas9 system to generate the knockout *col1a1* ± *365* mice (Fig. 1A). Since the exon 1-exon 2 junction splits the codon for amino acid 26 of pro-α1(I) chain [20], a substantially truncated peptide would produce as a result the frameshift mutation and premature termination at the 36th amino acid (Fig. 1B). Heterozygous mice was identified by PCR 2 weeks following birth and the result was shown in Fig. 1C. The mutant mice carrying a null *col1a1* allele had an obviously shorter band (594 bp) except the longer one (1623 bp), while the *wt* mice only produced 1623 bp band. We failed to gain any homozygous mice when the heterozygotes mated with each other, which probably was ascribed to the embryonic lethality of homozygous mutation. A growth deficiency reflected in weight gains became apparent soon post weaning in *col1a1* ± *365* mice, and the weight showed significantly less than that of the *wt* ones (Fig. 1D, E), similar to the manifestations of OI type I patients [21]. And during the study, none of spontaneous fractures were observed (SI Fig. 3).

3.2. Type I collagen expression

We checked the type I collagen expression of 8 weeks old mice. The results demonstrated that the protein level of pro-α1(I) in the femur remarkably reduced than that of normal mice (Fig. 2A). This proved the successful *col1a1* knockout and following global pro-α1(I) and collagen accumulation decrease. H&E stained sections of mutant femurs showed less and sparser trabeculae in spongy bones (Fig. 2B), implying an osteoporosis performance of mutant mice.

3.3. Micro-CT

Both the trabecular and cortical bone measurements for femurs of 8 and 20 weeks old mice were depicted in Fig. 3 and SI Fig. 2 respectively. The main distinctions lay in trabecular bones and there were no significant differences in cortical values (SI Fig. 2E) except the cortical bone area at the mid-diaphysis of the same aged mice. In 8 weeks old mice, the bone volume/total volume (Tb. BV/TV) of heterozygotes dropped about by half and the bone surface area/bone volume (Tb. BS/BV) nearly doubled compared to *wt* ones, which might be partly ascribed to the significantly reduced trabecular thickness (Tb. Th, Fig. 3B). Besides, both the reconstructed image and measurement values reflected much greater trabecular separation (Tb. Sp) of *col1a1* ± *365* mice, suggesting the lower connectivity and femur osteoporosis. Only a minute reduction in trabecular number (Tb. N) existed between the two genotypes (Fig. 3B). By 20 weeks, BV/TV, Tb. Sp and Tb. Th all got obvious increase in *col1a1* ± *365* mice, which were still remarkably lower than their normal littermates (Fig. 3B). And Tb. N of mutant femurs keeping the same level as 8 weeks was significantly less than the *wt* ones (Fig. 3B).

3.4. Bone mineralization and biomechanics

Bone mineral deposition is strongly associated with type I collagen level. As expected, both bone mineral density (BMD) and bone mineral content (BMC) of 8 and 20 weeks old *col1a1* ± *365* mice were significantly smaller than that of even-aged *wt* ones (Fig. 4A, B). Although the mineralization improved along with aging in mutant femurs, the difference got more apparent when compared to *wt* mice (Fig. 4B), which was different from the Mov-13 mice.

Collagen fibers make great contributions to bone mechanical properties. The biomechanical estimations indicated that the femur stress curves were distinct between the two types of mice either in 8 or 20 weeks (Fig. 4C, D). The *col1a1* ± *365* femurs bore a markedly smaller

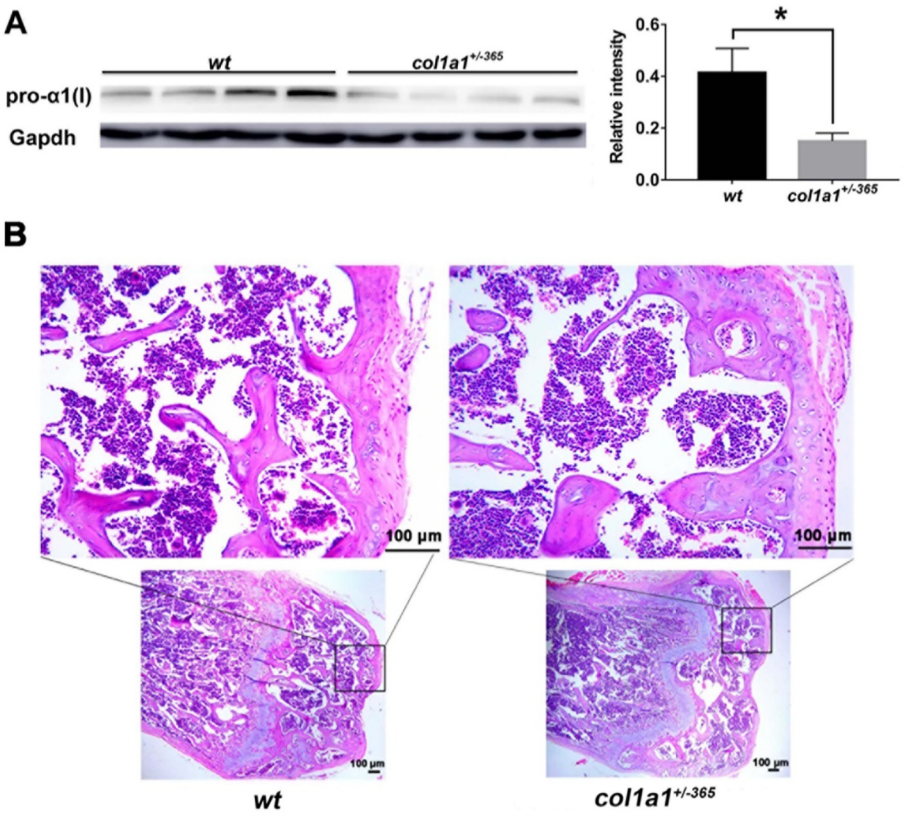

Fig. 2. Type I collagen expression and histology in femurs of 8 weeks old mice
A The femur pro-α1(I) expression tested by Western blot(n = 6). **B** H&E staining of femur sections from *wt* and *col1a1* ± *365* littermates (n = 6). The above images were higher-magnification views of the rectangular area of below images, respectively. *$p < 0.05$.

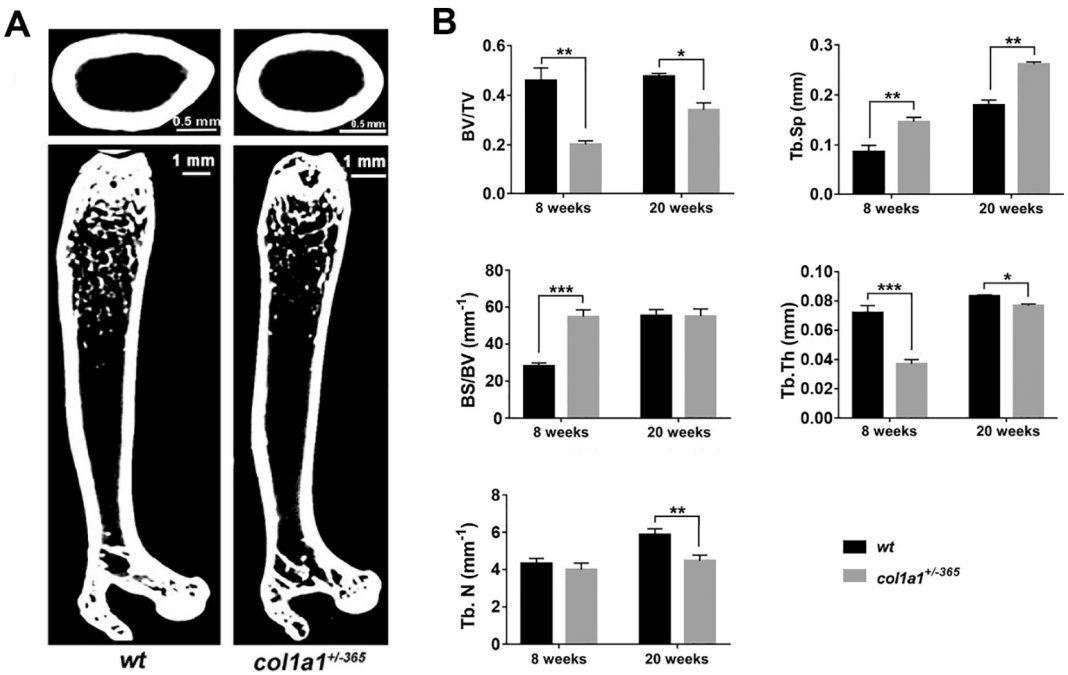

Fig. 3. Micro-CT measurements of 8 and 20 weeks old mice
A The 3D reconstructed images of cortical (above) and trabecular (below) bones of femurs from 8-week-old *wt* and *col1a1* $^{\pm}$ *365* mice. **B** The statistical analysis of trabecular microarchitecture parameters (n = 6 for each group). Bone Volume/tissue Volume (BV/TV), Trabecular Spacing (Tb.Sp, mm), Bone Surface Area/Bone Volume (BS/BV, 1/mm), Trabecular Thickness (Tb.Th, mm), Trabecular Number (Tb.N, 1/mm). *$p < 0.05$, **$p < 0.01$, ***$p < 0.005$.

maximum load and the post-yield displacement and plasticity were significantly reduced. Both the maximum load and stiffness arose in 20 weeks old mice, still, mutant femurs exhibited distinctly lowered maximum load and stiffness (Fig. 4E, F), unlike Mov-13 mice. Also, the Post-Yield Displacement, Post-Yield Energy and Work-to-Fracture of the two time points were determined, and the *col1a1* $^{\pm 365}$ mice exhibited remarkably smaller values compared with their peer control mice (Fig. 4G), which indicated that mutant bones failed in a more brittle manner.

3.5. Bone metabolism

The bone homeostasis is mainly maintained by balanced osteoblast osteogenesis and osteoclast resorption, which can be partly represented by the serum PINP and CTX-I levels respectively [22]. The obviously lower serum PINP (Fig. 5A) but higher CTX-I (Fig. 5B) concentration revealed that weakened collagen secretion and unusually active degradation existed in *col1a1* $^{\pm}$ *365* mice at the two time points. The PINP production obviously reduced, but the CTX-I level remained stable as *col1a1* $^{\pm}$ *365* mice grew up, indicating a sustained bone absorption. The continuously active osteoclasts might contribute to the sustained brittle bones of mutant mice. Besides, both the percentage and number of TRAP-positive osteoclasts on the trabecular surface significantly increased in *col1a1* $^{\pm}$ *365* trabecular bone compared to *wt* mice (Fig. 5C). All data here suggested that one null gene of *col1a1* broke bone metabolism equilibration and bone resorption creating accompanied with bone formation reducing might be responsible for bone loss of *col1a1* $^{\pm}$ *365* mice.

3.6. Osteogenic differentiation and Hippo/YAP signaling

Adipose-derived mesenchymal stem cells (ADSCs) are multipotent cells isolated from adipose tissue by a minimally invasive procedure. As similar with bone marrow mesenchymal stem cells (BMSCs), ADSCs have the capacity to differentiate into various cells of mesenchymal origin, including adipocytes, chondrocytes, myocytes and osteoblasts, when exposed to specific signals [23]. To further explore the potential impact of collagen alterations on bone formation, the osteogenic capacity of ADSCs was studied, and bone formation marker of femur were detected. The RNA expression of osteogenesis specific transcription factors *runx2* and *osterix* both significantly reduced in heterozygous femurs (Fig. 6A) and ADSCs $^{\pm}$ *365* (Fig. 7C) when compared with *wt* littermates. The obviously lighter ALP staining and significantly lowered ALP activity both existed in ADSCs $^{\pm}$ *365* (Fig. 7A, B). And the Bglap protein fell by about half in *col1a1* $^{\pm}$ *365* femurs (Fig. 6B), confirming the defect in osteogenesis. Since recent studies reported that YAP/TAZ plays an important role in osteogenic differentiation of BMSCs [24,25], YAP expression was examined. The results indicated that the protein level of YAP in mutant femurs reduced by about 60% (Fig. 6C). And the transcriptional expression of YAP/TAZ target genes including *ctgf* and *cyr61* all decreased distinctly (Fig. 6D). YAP immunofluorescent staining and the nuclear fluorescent intensity analysis of ADSCs^{wt} and ADSC $^{\pm}$ *365* treated without or with osteogenic induction medium for 3 days. Consistent with previous investigations [14,26], YAP mainly expressed in nucleus of ADSCs during osteogenic differentiation, most of which located in cytoplasm of the untreated cells (Fig. 7D). And the endonuclear YAP level of ADSCs $^{\pm}$ *365* was significantly lower than that of ADSCs^{wt} (Fig. 7D), suggesting that the reduced YAP level might be involved in the weakened osteogenesis and osteogenic capacity of *col1a1* mutant bones and ADSCs.

4. Discussion

The type I collagen, a triple helix consisted of two pro-α1(I) and one pro-α2(I) chains encoded by *COL1A1* and *COL1A2* genes respectively, constitutes the major components of extracellular matrix (ECM) [27–30]. Especially, the assembled collagen type I fibers with deposited minerals in bone matrix provide mechanical strength for bones, and any change in either the amount or organization of collagen fibers would make bones affected [28,30,31]. Osteogenesis imperfecta (OI) is such a congenital disorder mainly caused by abnormal collagen synthesis, and the typical manifestations include bone fragility, low bone mass,

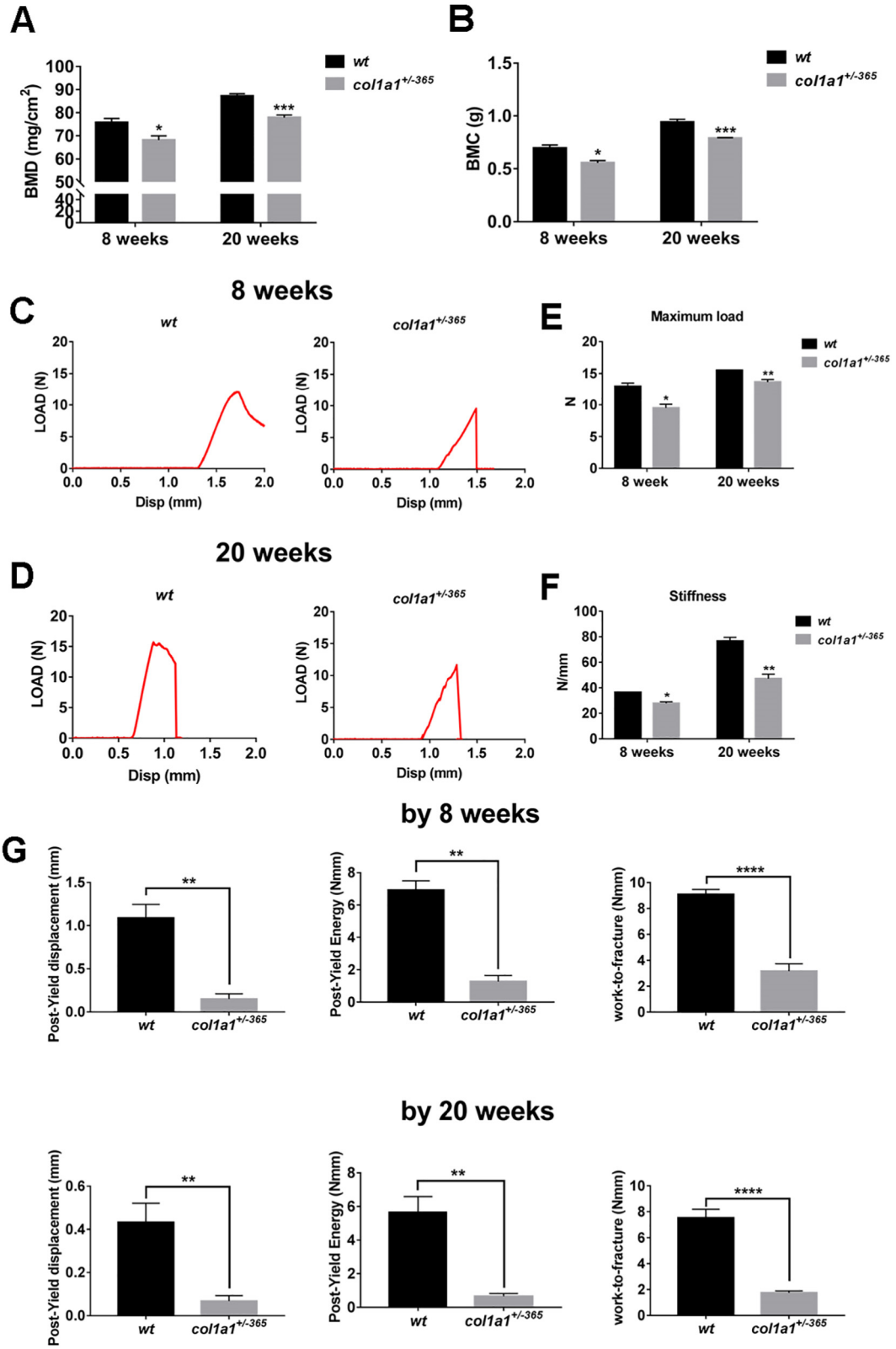

Fig. 4. Bone mineralization and biomechanics of 8 and 20 weeks old mice

A and **B** showed the BMD (bone mineral density) and BMC (bone mineral content) detected by DXA from the two kind of mice (n = 8 mice/group). **C** and **D** represented the load-displacement curves of femurs from mice. The biochemical properties were reflected by maximum load (**E**), stiffness (**F**), the Post-Yield Displacement (**G**), Post-Yield Energy (**G**) and Work-to-Fracture (**G**). $*p < 0.05$, $**p < 0.01$, $***p < 0.005$.

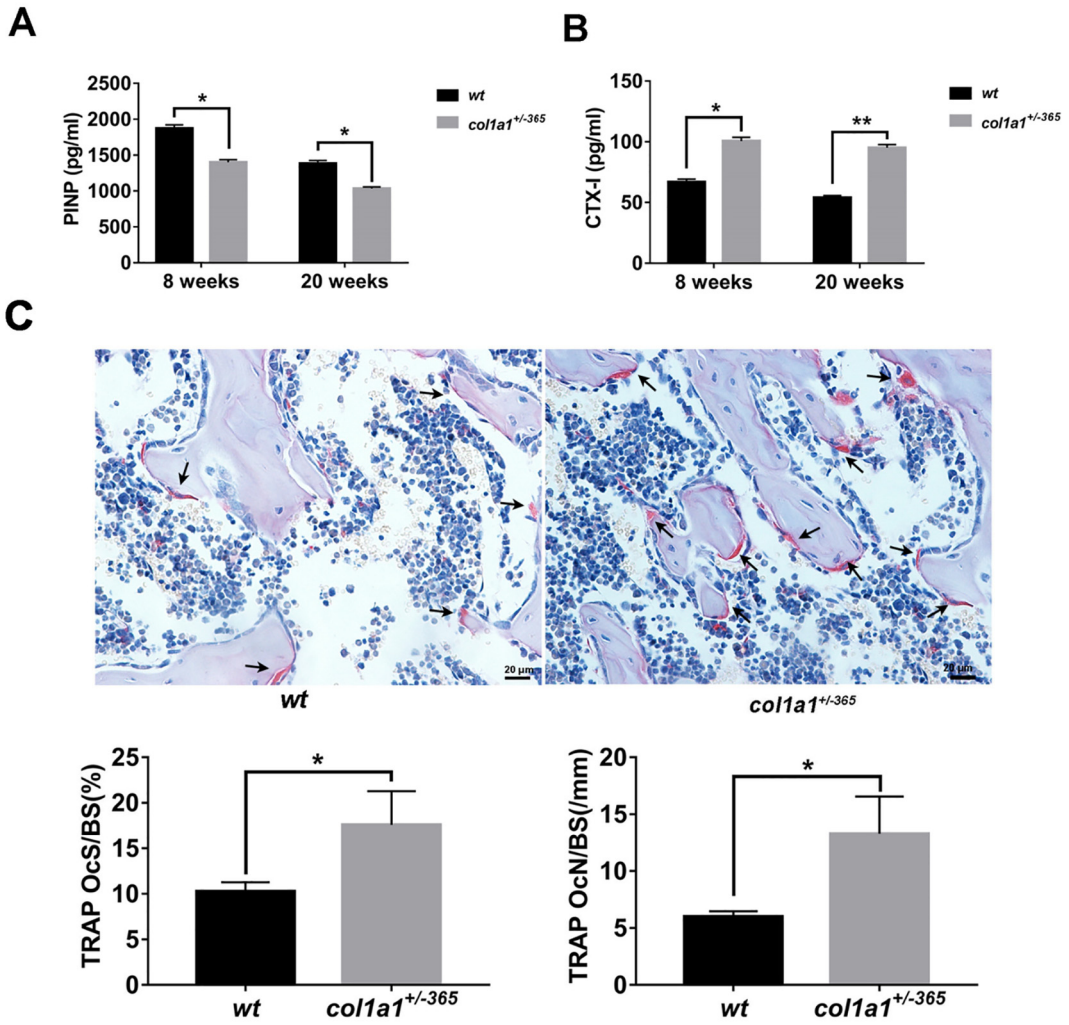

Fig. 5. Bone metabolism

The serum concentrations of P1NP **(A)** and CTX-I **(B)** (n = 8 mice/group) by 8 and 20 weeks. **C** Representative views of TRAP staining and TRAP-positive osteoclast counting of distal femur trabecular bone by 8 weeks. The black arrows indicated TRAP-positive osteoclasts. $TRAP^+OcS/BS$ (%): percentage of the TRAP-positive osteoclast in contact with trabecular surface, $TRAP^+OcN/BS$ (mm): number of TRAP-positive osteoclasts per millimeter of the trabecular surface. $*p < 0.05$, $**p < 0.001$.

skeletal deformity and short stature [2,32].

Genetic approaches greatly promote the research on OI pathogenesis especially the causing gene screening, and at least 17 genes have been found associated with different types of OI [1]. And the dominant mutations covering null and structural mutations in *COL1A1* and *COL1A2* genes are responsible for about 85% cases, among which a mild type I without bone deformities resulted from haploinsufficiency of *COL1A1* is the most prevalent type in patients [2,5,33].

Except the clinical observations, animal models also greatly extended the cellular and molecular findings of OI. Presently, there is only one OI type I model named Mov-13 (MOV $13^{+/-}$) strain that carries a provirus disrupting transcription initiation of pro-α1(I) [22,34]. While, we and other teams have reported that the degradation of mutant transcripts by Nonsense Mediated Decay (NMD) pathway and reduced synthesis of normal collagen caused OI type I [6,8,35].

To closely simulate clinical cases, the exon 2- exon 5 of *col1a1* gene (1029 bp in DNA, 365 nt in mRNA) was deleted using CRISPR/Cas9 system (Fig. 1), and the results showed that the type I collagen expression greatly reduced (Fig. 2A). Since type I collagen, the most abundant protein in organic matrix of bones, supplies the scaffold for mineral deposition and defines the size and distribution of apatite crystals together with non-collageneous proteins in the bone. And the lowered collagen synthesis will lead to a decreased mineralization in bones accompanied with bone mass and/or strength affected [5,36], which were proved by the micro-CT (Fig. 3) DXA (Fig. 4A, B) and biomechanical detection (Fig. 4C–G).

The *col1a1* $^{\pm}$ *365* mice showed some of the same characteristics with Mov-13 mice, such as the BMD, BMC and mechanical properties all reduced at 8 weeks (Fig. 4). But there were more difference between the two kinds of OI mice. The maximum load and mineralization of Mov-13 mice by 15 week recovered to the same level of wild mice [35]. While, the femurs of *col1a1* $^{\pm}$ *365* mice exhibited distinctly lower mineralization, maximum load and stiffness than their normal litters by 20 weeks (Fig. 4). We speculated that the different methods of constructing mouse models led to this result, but the mechanism needed further analysis.

Normal bone metabolism and homeostasis is maintained by coordinated cycles of bone formation and resorption, which are executed by osteoblasts and osteoclasts respectively [37–39]. Many studies indicated that OI patients and modeling animals showed hyperactive bone absorption and osteoclasts growth, which has been one intervention target in OI treatments [40–45]. Similar metabolic abnormities and significantly lowered osteogenesis also could be found in *col1a1* $^{\pm 365}$ mice (Fig. 5; Fig. 6A, B). The PINP content of mutant mice

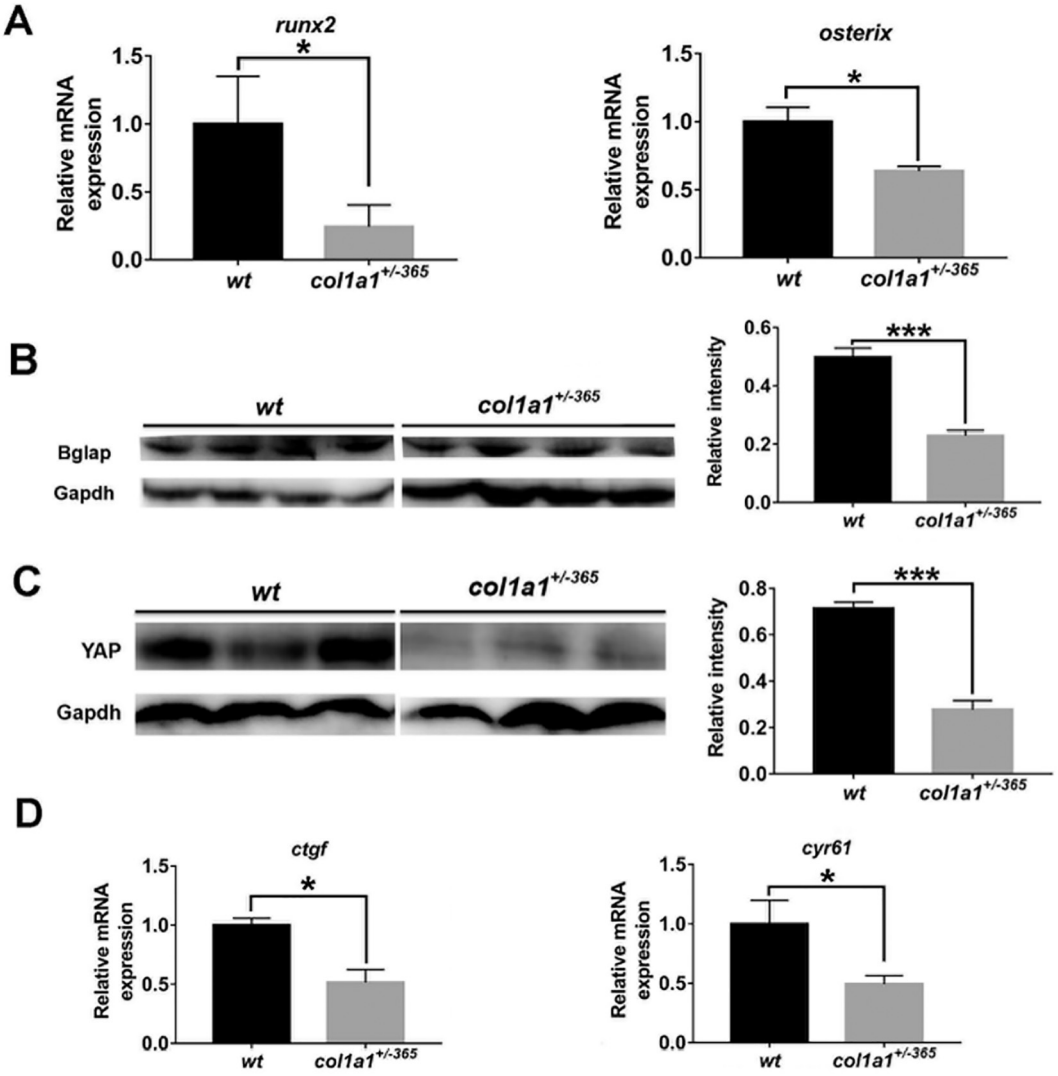

Fig. 6. The osteogenesis and YAP signaling in femurs of 8 weeks old mice
A The transcriptional expression of osteogenic transcription factors *runx2* and *osterix* in femurs. The protein level of Bglap (**B**, n = 6) and YAP (**C**, n = 6) in femurs. **D** the gene expression of YAP targeted genes *ctgf* and *cyr61* in Hippo/YAP signaling pathway. $*p < 0.05$, $***p < 0.005$.

significantly reduced than the *wt* controls at the two time points and it obviously declined as mice grew up (Fig. 5A), demonstrating osteogenesis defect. The CTX-I level of *col1a1* $^{\pm 365}$ mice clearly increased compared to the normal ones and remained stable (Fig. 5B), suggesting a sustained bone absorption. The continuously active osteoclasts might contribute to the sustained brittle bones of mutant mice.

BMSCs are the source of osteoblasts and it has been reported that the osteogenic capacity of OI backgrounded BMSCs decreases obviously [46], but the latent mechanisms are still poorly understood. Similarly, ADSCs $^{\pm}$ *365* also performed weakened osteoblast differentiation (Fig. 7A–C), which has not been reported yet in relative studies. Recent works have focused on the Hippo/YAP pathway in osteogenesis of BMSCs [26,47]. We tested the femoral YAP expression and the results showed a largely dropped YAP level and the distinct transcriptional reductions of downstream genes including *runx2* [48–50] (Fig. 6A, Fig. 7C), *ctgf and cyr61* [47,51] (Fig. 6D). The endonuclear YAP expression also reduced significantly in ADSCs $^{\pm}$ *365* incubated with osteogenic induction medium (Fig. 7D). In addition, most of ADSCs $^{\pm}$ *365* cultured on collagen type I coated dishes exhibited nuclear YAP location and effectively increased *runx2* expression (SI Fig. 4). These results all demonstrated that YAP downregulation and reduced nuclear level was partly at least relative to osteoblast differentiation of ADSCs $^{\pm}$ *365*. This was the first evidence of the roles of Hippo/YAP signaling in osteogenic differentiation of OI derived models and mesenchymal stem cells. Still, the detailed pathway from type I collagen to YAP and downstream targets involved in osteogenesis needed more in-depth investigations.

5. Conclusions

In the present study, the *col1a1* $^{\pm 365}$ strain with *col1a1* exon 2-exon 5 deletion by CRISPR/Cas9 system was designed to provide a novel transgenic model to mimic OI type I from genotype to phenotype. The heterozygotes manifested remarkably reduced type I collagen expression, bone mineralization and mechanical properties until 20 weeks old, indicating stable bone brittleness in spite of few improvement existed in some indicators as the mice grew up. YAP downregulation was associated with reduced bone osteogenesis and reduced osteogenic capacity of ADSCs $^{\pm}$ *365*, but the underlying mechanisms remained to be further clarified.

Declaration of Competing Interest

The authors do not have any conflict of interests.

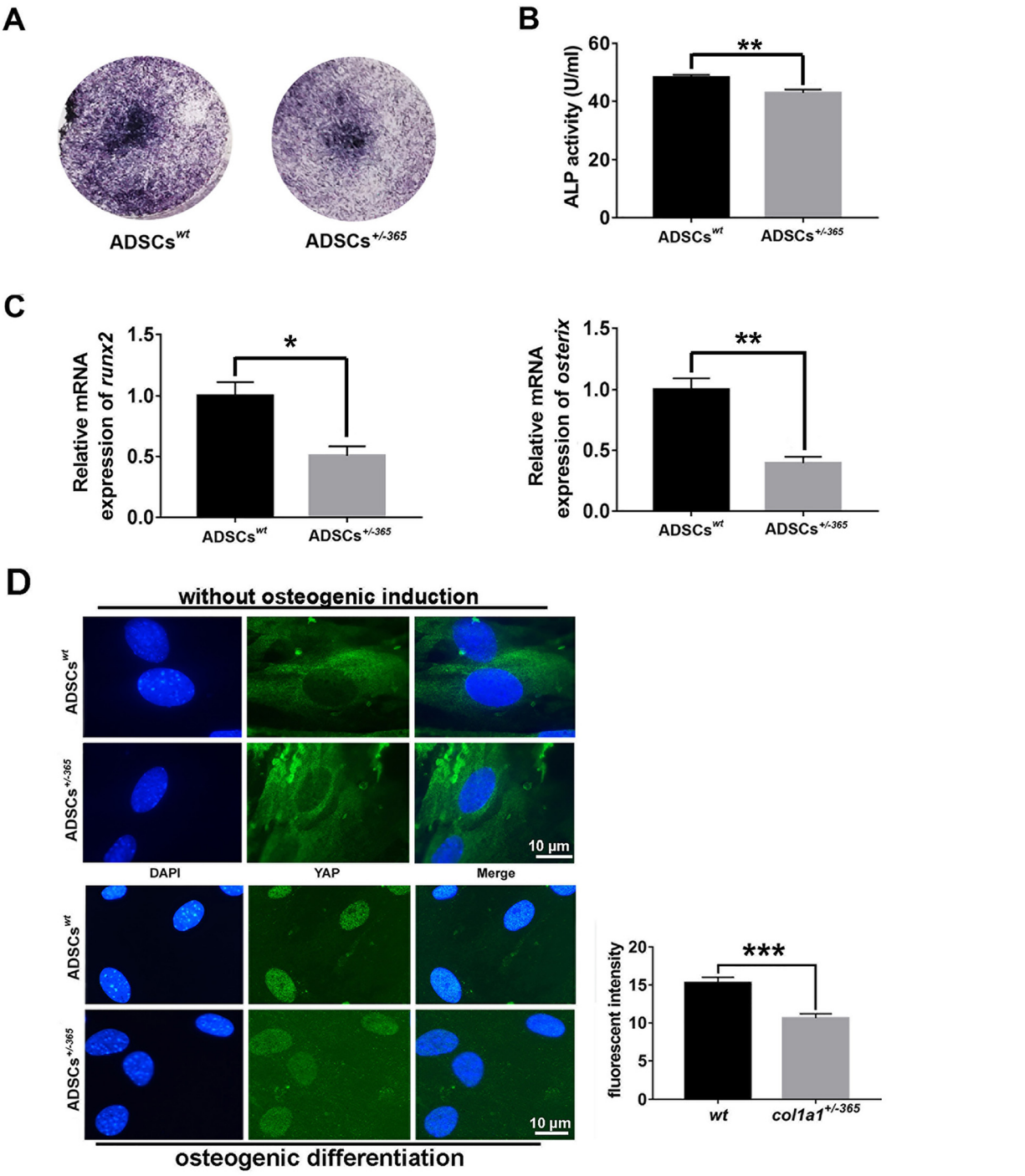

Fig. 7. The osteogenic differentiation potential and YAP signaling in ADSCs
A ALP staining of ADSCs^{wt} (n = 4) and ADSC $^{\pm}$ *365* (n = 4) treated with osteogenic induction medium for 14 days. **B** The ALP activity in supernatants of ADSCs^{wt} (n = 8) and ADSC $^{\pm}$ *365* (n = 8) under osteogenic induction by 14 days. **C** The mRNA level of osteogenic transcription factors *runx2* and *osterix* of ADSCs^{wt} (n = 6) and ADSC $^{\pm}$ *365* (n = 6) under osteogenic induction by 14 days. **D** YAP immunofluorescent staining and the nuclear fluorescent intensity analysis of ADSCs^{wt} (n = 5) and ADSC $^{\pm}$ *365* (n = 5) treated without or with osteogenic induction medium for 3 days. *p vs. ADSCs^{wt} < 0.05, **p vs. ADSCs^{wt} < 0.01, ***p vs. ADSCs^{wt} < 0.005.

Acknowledgments

The present work was supported by the grant from National Key Research and Development Program of China (2017YFC1001900 and 2017YFC1001904), Tianjin Science and Technology Support Program (16YFZCSY00900) and Natural Science Foundation of China for Young Scholars (81501386).

Appendix A. Supplementary data

Supplementary data to this article can be found online at https://doi.org/10.1016/j.bone.2019.07.021.

References

[1] A. Forlino, J.C. Marini, Osteogenesis imperfecta, Lancet 387 (10028) (2016)

1657–1671. Apr 16.
[2] J.C. Marini, A. Forlino, H.P. Bachinger, N.J. Bishop, P.H. Byers, A. Paepe, et al., Osteogenesis imperfecta, Nat. Rev. Dis. Primers 3 (Aug 18 2017) 17052.
[3] F.S. van Dijk, P.H. Byers, R. Dalgleish, F. Malfait, A. Maugeri, M. Rohrbach, et al., EMQN best practice guidelines for the laboratory diagnosis of osteogenesis imperfecta, Eur. J. Hum. Genet. 20 (1) (2012) 11–19 Jan.
[4] C.M. Jacobsen, M.A. Schwartz, H.J. Roberts, K.E. Lim, L. Spevak, A.L. Boskey, et al., Enhanced Wnt signaling improves bone mass and strength, but not brittleness, in the Col1a1(+/mov13) mouse model of type I osteogenesis imperfecta, Bone 90 (2016) 127–132 Sep.
[5] R. Morello, Osteogenesis imperfecta and therapeutics, Matrix Biol. 71–72 (2018) 294–312 Oct.
[6] J.H. Wang, X.Z. Ren, X. Bai, T.K. Zhang, Y. Wang, K.Q. Li, et al., Identification of gene mutation in patients with osteogenesis imperfect using high resolution melting analysis, Sci. Rep. 5 (2015) Aug 26.
[7] < Premature chain termination is a unifying mechanism for COL1A1 null alleles in osteogenesis imperfecta type I cell strains.pdf > .
[8] G. Bardai, E. Lemyre, P. Moffatt, T. Palomo, F.H. Glorieux, J. Tung, et al., Osteogenesis imperfecta type I caused by COL1A1 deletions, Calcif. Tissue Int. 98 (1) (2016) 76–84 Jan.
[9] A. Forlino, W.A. Cabral, A.M. Barnes, J.C. Marini, New perspectives on osteogenesis imperfecta, Nat. Rev. Endocrinol. 7 (9) (Jun 14 2011) 540–557.
[10] D. Jahner, R. Jaenisch, Retrovirus-induced de novo methylation of flanking host sequences correlates with gene inactivity, Nature 315 (6020) (1985) 594–597 Jun 13-19.
[11] S. Hartung, R. Jaenisch, M. Breindl, Retrovirus insertion inactivates mouse alpha 1(I) collagen gene by blocking initiation of transcription, Nature 320 (6060) (Mar 27-Apr 2 1986) 365–367.
[12] J. B, K.J. J, M.K. M, R. J, J.L. K, S.A. G, A murine skeletal adaptation that significantly increases cortical bone mechanical properties. Implications for human skeletal fragility, J. Clin. Invest. 92 (4) (1993) 1697–1705 Oct.
[13] L. Xiang, H. Yu, X. Zhang, B. Wang, Y. Yuan, Q. Zhang, et al., The versatile hippo pathway in oral-maxillofacial development and bone remodeling, Dev. Biol. 440 (2) (Aug 15 2018) 53–63.
[14] C.D. Kegelman, D.E. Mason, J.H. Dawahare, D.J. Horan, G.D. Vigil, S.S. Howard, et al., Skeletal cell YAP and TAZ combinatorially promote bone development, FASEB J. 32 (5) (May 2018) 2706–2721.
[15] J.X. Pan, L. Xiong, K. Zhao, P. Zeng, B. Wang, F.L. Tang, et al., YAP promotes osteogenesis and suppresses adipogenic differentiation by regulating beta-catenin signaling, Bone Res. 6 (2018) 18.
[16] J.R. Maddox, X. Liao, F. Li, C. Niyibizi, Effects of culturing on the stability of the putative murine adipose derived stem cells markers, Open Stem Cell J. 1 (Jan 1 2009) 54–61.
[17] Q. Ma, J. Yang, X. Huang, W. Guo, S. Li, H. Zhou, et al., Poly(Lactide-co-Glycolide)-Monomethoxy-poly-(polyethylene glycol) nanoparticles loaded with melatonin protect adipose-derived stem cells transplanted in infarcted heart tissue, Stem Cells 36 (4) (2018) 540–550. Apr.
[18] K.J. Jepsen, M.J. Silva, D. Vashishth, X.E. Guo, M.C.H. van der Meulen, Establishing biomechanical mechanisms in mouse models: practical guidelines for systematically evaluating phenotypic changes in the Diaphyses of Long bones, J. Bone Miner. Res. 30 (6) (2015) 951–966 Jun.
[19] A. Colberg, R. Frazine, K. Sampson, M.L. Villarraga, P.J. Didier, Mechanical properties of rhesus femoral cortical bone as determined by three-point bending and ultrasound tests, FASEB J. 13 (5) (Mar 15 1999) A912–A.
[20] P. Bornstein, V. Walsh, J. Tullis, E. Stainbrook, J.F. Bateman, S.G. Hormuzdi, The globular domain of the proalpha 1(I) N-propeptide is not required for secretion, processing by procollagen N-proteinase, or fibrillogenesis of type I collagen in mice, J. Biol. Chem. 277 (4) (Jan 25 2002) 2605–2613.
[21] A.M. Sepulveda, C.V. Terrazas, J. Saez, M.L. Reyes, Vertebral fractures in children with type I osteogenesis imperfecta, Rev. Chil. Pediatr. 88 (3) (2017) 348–353 Jun.
[22] Z. Xie, H.J. Yu, X.W. Sun, P. Tang, Z.W. Jie, S. Chen, et al., A novel Diterpenoid suppresses Osteoclastogenesis and promotes osteogenesis by inhibiting Ifrd1-mediated and IB-mediated p65 nuclear translocation, J. Bone Miner. Res. 33 (4) (2018) 667–678. Apr.
[23] S. Mohamed-Ahmed, I. Fristad, S.A. Lie, S. Suliman, K. Mustafa, H. Vindenes, et al., Adipose-derived and bone marrow mesenchymal stem cells: a donor-matched comparison, Stem Cell Res Ther (Jun 19 2018) 9.
[24] S. Dupont, Role of YAP/TAZ in cell-matrix adhesion-mediated signalling and mechanotransduction, Exp. Cell Res. 343 (1) (Apr 10 2016) 42–53.
[25] K.A. Jansen, P. Atherton, C. Ballestrem, Mechanotransduction at the cell-matrix interface, Semin. Cell Dev. Biol. 71 (2017) 75–83 Nov.
[26] Y. Tang, S.J. Weiss, Snail/slug-YAP/TAZ complexes cooperatively regulate mesenchymal stem cell function and bone formation, Cell Cycle 16 (5) (2017) 399–405 Mar 4.
[27] L.E. Niklason, Understanding the extracellular matrix to enhance stem cell-based tissue regeneration, Cell Stem Cell 22 (3) (Mar 1 2018) 302–305.
[28] A.K. Nair, A. Gautieri, S.W. Chang, M.J. Buehler, Molecular mechanics of mineralized collagen fibrils in bone, Nat. Commun. 4 (2013) Apr.
[29] X. Liu, X. Long, W. Liu, Y. Zhao, T. Hayashi, M. Yamato, et al., Type I collagen induces mesenchymal cell differentiation into myofibroblasts through YAP-induced TGF-beta1 activation, Biochimie 150 (2018) 110–130 Jul.
[30] C. Wittkowske, G.C. Reilly, D. Lacroix, C.M. Perrault, In vitro bone cell models: impact of fluid shear stress on bone formation, Front. Bioeng. Biotechnol. 4 (2016) 87.
[31] K.C. Murphy, A.I. Hoch, J.N. Harvestine, D.J. Zhou, J.K. Leach, Mesenchymal stem cell spheroids retain osteogenic phenotype through alpha(2)beta(1) signaling, Stem Cells Transl. Med. 5 (9) (2016) 1229–1237 Sep.
[32] S. Tournis, A.D. Dede, Osteogenesis imperfecta - A clinical update, Metab. Clin. Exp. 80 (2018) 27–37 Mar.
[33] L.N. Veilleux, A. Pouliot-Laforte, M. Lemay, M.S. Cheung, F.H. Glorieux, F. Rauch, The functional muscle-bone unit in patients with osteogenesis imperfecta type I, Bone. 79 (2015) 52–57 Oct.
[34] J. Saban, M.A. Zussman, R. Havey, A.G. Patwardhan, G.B. Schneider, D. King, Heterozygous oim mice exhibit a mild form of osteogenesis imperfecta, Bone 19 (6) (1996) 575–579 Dec.
[35] J. Bonadio, T.L. Saunders, E. Tsai, S.A. Goldstein, J. Morris-Wiman, L. Brinkley, et al., Transgenic mouse model of the mild dominant form of osteogenesis imperfecta, Proc. Natl. Acad. Sci. U. S. A. 87 (18) (1990) 7145–7149 Sep.
[36] R. Florencio-Silva, G.R.D. Sasso, E. Sasso-Cerri, M.J. Simoes, P.S. Cerri, Biology of bone tissue: structure, function, and factors that influence bone cells, Biomed. Res. Int. 2015 (2015) 421746.
[37] Y.J. Han, X.L. You, W.H. Xing, Z. Zhang, W.G. Zou, Paracrine and endocrine actions of bone-the functions of secretory proteins from osteoblasts, osteocytes, and osteoclasts, Bone Res. 6 (2018) May 24.
[38] I.R. Indran, R.L. Liang, T.E. Min, E.L. Yong, Preclinical studies and clinical evaluation of compounds from the genus Epimedium for osteoporosis and bone health, Pharmacol. Ther. 162 (2016) 188–205 Jun.
[39] R. Baron, M. Kneissel, WNT signaling in bone homeostasis and disease: from human mutations to treatments, Nat. Med. 19 (2) (2013) 179–192 Feb.
[40] H. Hoyer-Kuhn, C. Netzer, O. Semler, Osteogenesis imperfecta: pathophysiology and treatment, Wien. Med. Wochenschr. 165 (13–14) (2015) 278–284 Jul.
[41] J.E. Perosky, B.M. Khoury, T.N. Jenks, F.S. Ward, K. Cortright, B. Meyer, et al., Single dose of bisphosphonate preserves gains in bone mass following cessation of sclerostin antibody in Brtl/plus osteogenesis imperfecta model, Bone 93 (2016) 79–85 Dec.
[42] I. Vuorimies, H. Arponen, H. Valta, O. Tiesalo, M. Ekholm, H. Ranta, et al., Timing of dental development in osteogenesis imperfecta patients with and without bisphosphonate treatment, Bone 94 (2017) 29–33 Jan.
[43] T.E. Uveges, P. Collin-Osdoby, W.A. Cabral, F. Ledgard, L. Goldberg, C. Bergwitz, et al., Cellular mechanism of decreased bone in Brtl mouse model of OI: imbalance of decreased osteoblast function and increased osteoclasts and their precursors, J. Bone Miner. Res. Off. J. Am. Soc. Bone Miner. Res. 23 (12) (Dec 2008) 1983–1994.
[44] D. Gatti, F. Antoniazzi, R. Prizzi, V. Braga, M. Rossini, L. Tato, et al., Intravenous neridronate in children with osteogenesis imperfecta: a randomized controlled study, J. Bone Miner. Res. Off. J. Am. Soc. Bone Miner. Res. 20 (5) (2005) 758–763 May.
[45] A.G. Feehan, M.R. Zacharin, A.S. Lim, P.J. Simm, A comparative study of quality of life, functional and bone outcomes in osteogenesis imperfecta with bisphosphonate therapy initiated in childhood or adulthood, Bone 113 (2018) 137–143. Aug.
[46] R. Gioia, C. Panaroni, R. Besio, G. Palladini, G. Merlini, V. Giansanti, et al., Impaired Osteoblastogenesis in a murine model of dominant osteogenesis imperfecta: a new target for osteogenesis imperfecta pharmacological therapy, Stem Cells 30 (7) (2012) 1465–1476 Jul.
[47] H.W. Park, Y.C. Kim, B. Yu, T. Moroishi, J.S. Mo, S.W. Plouffe, et al., Alternative Wnt signaling activates YAP/TAZ, Cell 162 (4) (Aug 13 2015) 780–794.
[48] J.H. Xiong, M. Almeida, C.A. O'Brien, The YAP/TAZ transcriptional co-activators have opposing effects at different stages of osteoblast differentiation, Bone 112 (2018) 1–9 Jul.
[49] W. Hong, K.L. Guan, The YAP and TAZ transcription co-activators: key downstream effectors of the mammalian hippo pathway, Semin. Cell Dev. Biol. 23 (7) (2012) 785–793 Sep.
[50] X.Z. Jing, J. Wang, W.F. Yin, G.H. Li, Z. Fang, W.T. Zhu, et al., Proliferation and differentiation of rat adipose-derived stem cells are regulated by yes-associated protein, Int. J. Mol. Med. 42 (3) (2018) 1526–1536 Sep.
[51] W.X. Zhang, J.J. Xu, J.H. Li, T. Guo, D. Jiang, X. Feng, et al., The TEA domain family transcription factor TEAD4 represses murine adipogenesis by recruiting the cofactors VGLL4 and CtBP2 into a transcriptional complex, J. Biol. Chem. 293 (44) (2018) 17119–17134 Nov 2.